Orbital pacing of carbon fluxes by a ∼9-My eccentricity cycle during the Mesozoic

Mathieu Martinez[a,b] **and Guillaume Dera**[c,1]

[a]Laboratoire des Fluides Complexes et Leurs Réservoirs, UMR 5150, CNRS, Total, Université de Pau et des pays de l'Adour, 64013 Pau, France; [b]Center for Marine Environmental Sciences, Universität Bremen, 28359 Bremen, Germany; and [c]Géosciences Environnement Toulouse, UMR 5563, CNRS, Institut de Recherche pour le Développement, Université Paul Sabatier, 31400 Toulouse, France

Edited by Paul E. Olsen, Columbia University, Palisades, NY, and approved July 16, 2015 (received for review October 17, 2014)

Eccentricity, obliquity, and precession are cyclic parameters of the Earth's orbit whose climatic implications have been widely demonstrated on recent and short time intervals. Amplitude modulations of these parameters on million-year time scales induce "grand orbital cycles," but the behavior and the paleoenvironmental consequences of these cycles remain debated for the Mesozoic owing to the chaotic diffusion of the solar system in the past. Here, we test for these cycles from the Jurassic to the Early Cretaceous by analyzing new stable isotope datasets reflecting fluctuations in the carbon cycle and seawater temperatures. Our results document a prominent cyclicity of ∼9 My in the carbon cycle paced by changes in the seasonal dynamics of hydrological processes and long-term sea level fluctuations. These paleoenvironmental changes are linked to a great eccentricity cycle consistent with astronomical solutions. The orbital forcing signal was mainly amplified by cumulative sequestration of organic matter in the boreal wetlands under greenhouse conditions. Finally, we show that the ∼9-My cycle faded during the Pliensbachian, which could either reflect major paleoenvironmental disturbances or a chaotic transition affecting this cycle.

orbital cycles | carbon cycle | paleoclimate | eustatism | Mesozoic

The calculation of the Earth's orbital parameters is crucial to identifying the natural effects of periodic changes in insolation (i.e., Milankovitch cycles) on the ongoing evolution of climate (1). Whereas the periodicity of these orbital cycles is well documented for the Quaternary (i.e., ∼95,000 and ∼405,000 y for eccentricity, ∼41,000 y for obliquity, and ∼19,000 and ∼23,000 y for precession) (2), numerical integration of orbital parameters through geological time predicts the existence of million-year periodicities manifested as amplitude modulations (AM) of shorter cycles (3, 4). Spectral analyses applied to sedimentary records covering large intervals of the Phanerozoic confirm these "grand orbital cycles" and demonstrate their key role in the pacing of climate changes and carbon transfers at million-year time scales (5, 6). Much attention has been given to the 2.4-My eccentricity period and to the 1.2-My obliquity period, which are linked to gravitational interactions between the Earth and Mars. Currently, they experience a 1:2 resonance (3–5), but this resonance has been identified as a major source of chaos in the past inner Solar System (7), so that the 2.4-My eccentricity cycle would be expected to experience chaotic transitions during the Mesozoic (8). It is difficult to predict when these chaotic transitions occurred. Whereas individual repetitions of the ∼2.4-My cycle range from 2.0 to 2.9 My in the Cenozoic (9), cyclostratigraphic studies suggest that this period strongly fluctuated from maximal values of ∼3.45 My during the Permian (10) to values ranging from ∼1.5–2.9 My during the Mesozoic (8, 11–13).

A ∼9-My cycle was recently reported in the sedimentary and geochemical signals of the Cenozoic, Late Cretaceous, and Triassic (14–16). These periodic patterns would correspond to secular climate changes (and carbon transfers) paced by a long eccentricity cycle, which results from amplitude modulation of the ∼2.4-My cycle (14). If stable, this ∼9-My astronomical cycle would constitute a useful tool for improving both the durations of stages in the geological time scale and astronomical solutions before 50 Ma. However, recent studies suggest that tectonic, volcanic, or eustatic factors may have affected its expression (14). Because of its link to the unstable 2.4-My cycle, it is also possible that the ∼9-My cycle experienced chaotic transitions through time, but no evidence has been presented to confirm this hypothesis (8).

Here, we explore the temporal expression, the origin, and the consequences of the ∼9-My orbital cycle from the Early Jurassic to the Early Cretaceous, a key period that links previous literature results (14–16). For this purpose, we apply spectral analyses to new time series of carbon and oxygen isotope data spanning 73.6 My from the Sinemurian (197.03 Ma) to the Aptian (123.43 Ma) (*Materials and Methods*). The isotopic values, which record fluctuations in the carbon cycle and seawater temperatures, are from well-preserved European belemnite rostra, which lived in tropical Tethyan seas prone to astroclimatic influences (11, 17, 18) (Fig. 1). Because belemnites were nektobenthic cephalopods supposed to precipitate their rostra in equilibrium with ambient seawater, it is assumed that the isotopic oscillations mainly reflect temperature changes and fluctuations in the dissolved inorganic carbon (DIC) composition of epicontinental seawaters from ∼100 to ∼250 m in depth (19). Even if interspecific differences in metabolism, feeding behavior, or water depth may interfere with the isotopic climate response on short time scales (20), we suggest that the turnover of species through time has little to no influence on the long-term periodic patterns.

Results

The power spectra of the $\delta^{13}C$ and $\delta^{18}O$ series shown in Fig. 2 are calculated after implementation of age-error simulations, to test the influence of geological time scale uncertainties on the robustness of spectral peaks (*Materials and Methods*). The spectrum of

Significance

The Milankovitch cycles are orbitally paced variations in insolation that drove periodic climate changes on Earth at the scale of tens to hundreds of thousands years. Longer "grand orbital cycles" also exist, but their impacts on paleoclimate dynamics are not well documented for pre-Cenozoic times. Here we tackle this issue by analyzing the stable isotope fluctuations recorded by fossil cephalopods throughout the Jurassic–Early Cretaceous interval. We document a periodicity of ∼9 My in the carbon cycle, except from 190 to 180 Ma when disturbances occurred. This orbital forcing affected carbon transfers by modulating the hydrological processes and sea-level changes. In summary, this ∼9-My orbital cycle is an important metronome of the greenhouse climate dynamics.

Author contributions: M.M. and G.D. designed research, performed research, contributed new reagents/analytic tools, analyzed data, and wrote the paper.

The authors declare no conflict of interest.

This article is a PNAS Direct Submission.

[1]To whom correspondence should be addressed. Email: guillaume.dera@get.obs-mip.fr.

This article contains supporting information online at www.pnas.org/lookup/suppl/doi:10.1073/pnas.1419946112/-/DCSupplemental.

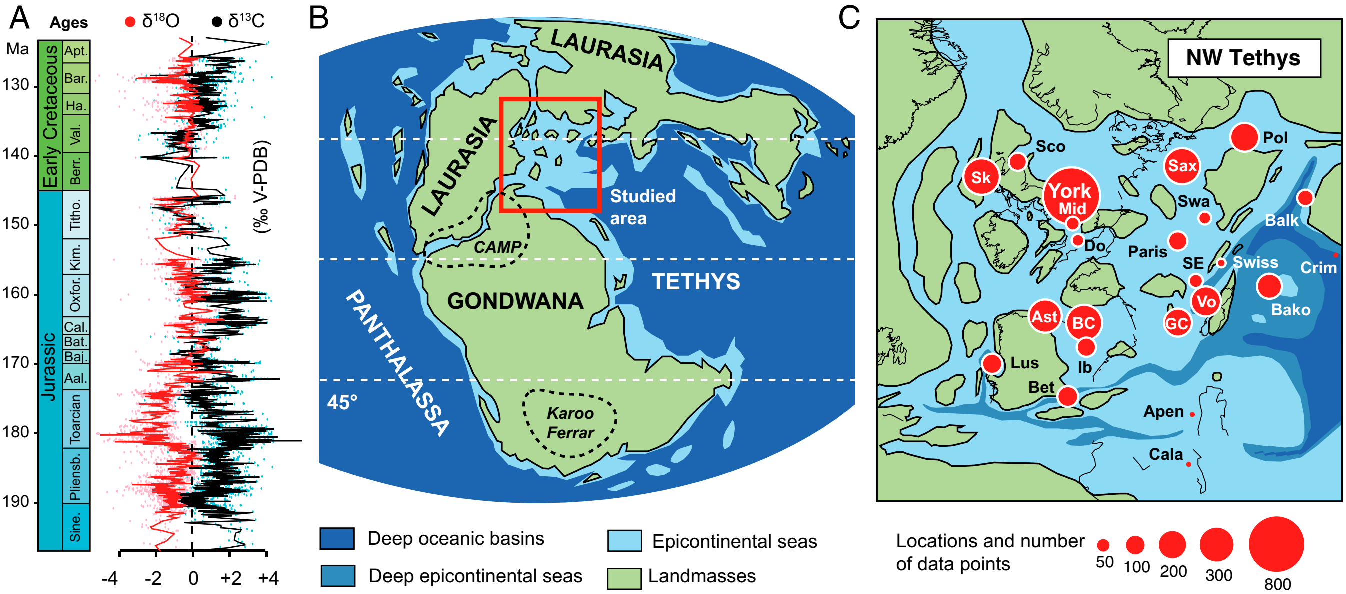

Fig. 1. Compilation of $\delta^{13}C$ and $\delta^{18}O$ data (*A*) measured on NW Tethyan belemnites represented in their global (*B*) and regional (*C*) paleogeographic contexts. (*B*) Modified from ref. 27, with permission from Elsevier and courtesy of Ron Blakey (Colorado Plateau Geosystems). (*C*) Image courtesy of the Commission of the Geological Map of the World (57). The smoothed isotopic curves are LOWESS regressions with respective coefficients of 0.0016313 and 0.0016667 for $\delta^{18}O$ and $\delta^{13}C$ data. Aal, Aalenian; Apen, Apennines; Apt, Aptian; Ast, Asturias; Baj, Bajocian; Bako, Bakony and Gerecse Mountains; Bar, Barremian; Bat, Bathonian; BC, Basque–Cantabrian Basin; Berr, Berriasian; Bet, Betic and Subbetic basins; Cal, Callovian; Cala, Calabria; Crim, Crimea; Do, Dorset; GC, Grands Causses Basin; Ha, Hauterivian; Ib, Iberian range; Kim, Kimmeridgian; Lus, Lusitanian Basin; Mid, Midland Platform; Oxfor, Oxfordian; Paris: east and northeast of the Paris Basin; Pliensb, Pliensbachian; Pol, Polish Jura Chain; Sax, Lower Saxony Basin; Sco, Northeastern Scotland; SE, Sud-Est Basin; Sine, Sinemurian; Sk, Isle of Skye; Swa, Swabian Basin; Swiss, Swiss Jura Chain; Titho, Tithonian; Val, Valanginian; Vo, Vocontian Basin; and York, Yorkshire.

the $\delta^{13}C$ series shows one main peak at 9.1 My (Fig. 2*A*), whereas that of the $\delta^{18}O$ series shows two main peaks at 11.7 and 5 My (Fig. 2*B*). These results are not dependent of smoothing method (Fig. S1). Nevertheless, only the peak of 9.1 My is stable whatever the detrending method used (Figs. S2 and S3) and exceeds the 95% Bonferroni-corrected confidence level in the robust red-noise fit and in LOWSPEC tests (Fig. S4), even after having tested the influence of temporal uncertainties in the geological time scale (21) (Fig. S5). On the filtered series and the spectrogram (Fig. 3 *C* and *H*), the 9.1-My peak seems to be a genuine high-amplitude cycle in the $\delta^{13}C$ series, having a strong power from the Sinemurian to the Early Aptian, and exceeding the 95% confidence level in the evolutive harmonic multitaper method (MTM) F-test. This period displays fluctuations from 7.9 My in the Bajocian to 10.1 My in the Berriasian, as well as a bifurcation from 190 to 180 Ma (Fig. 3*H*), so that this cycle does not have a purely harmonic behavior and does not exceed the 95% confidence level in the MTM F-test (Fig. S5). A peak of ∼1.9 My, exceeding the 95% confidence level in the evolutive harmonic F-test, also occurs but fails in the red-noise tests implementing Bonferroni corrections.

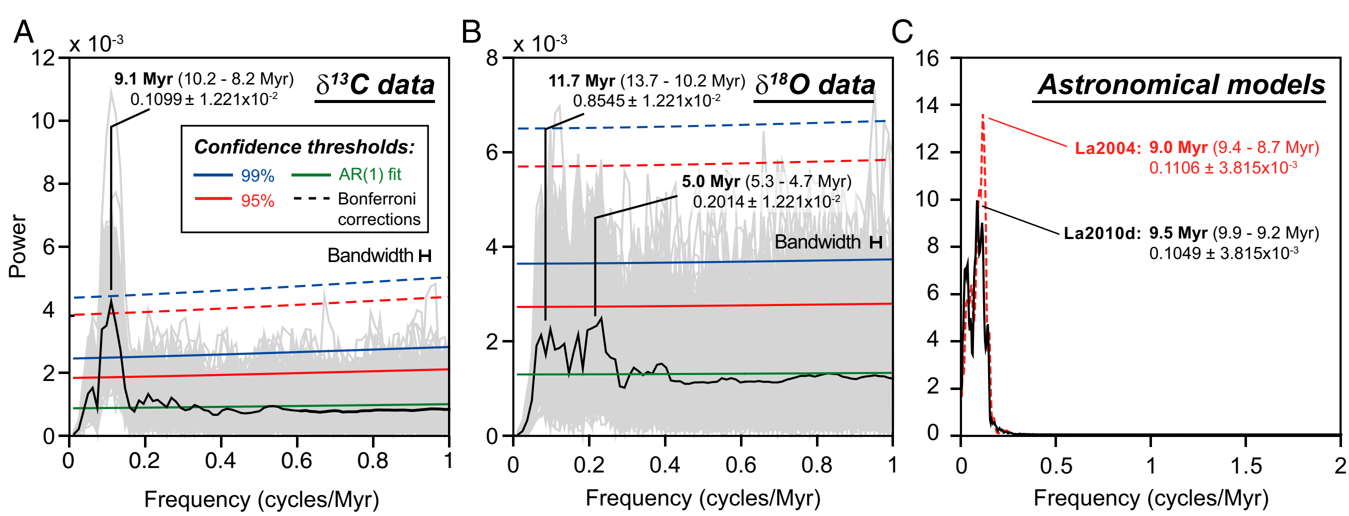

Fig. 2. The 2π-multitaper LOWSPEC-treated spectra of belemnite $\delta^{13}C$ (*A*) and $\delta^{18}O$ (*B*) time series. (*C*) The 2π-multitaper spectrum of the amplitude modulation of the 2.4-My band from the astronomical models (i.e., La2004 and La2010d) (3, 4) over the studied interval. The spectra shown in *A* and *B* were performed after running 1,000 Monte-Carlo age-random simulations. The gray lines represent the spectra of the 1,000 simulations and the black line represents the average spectrum. Only the 9.1-My cycle is significant with respect to Bonferroni-corrected confidence thresholds.

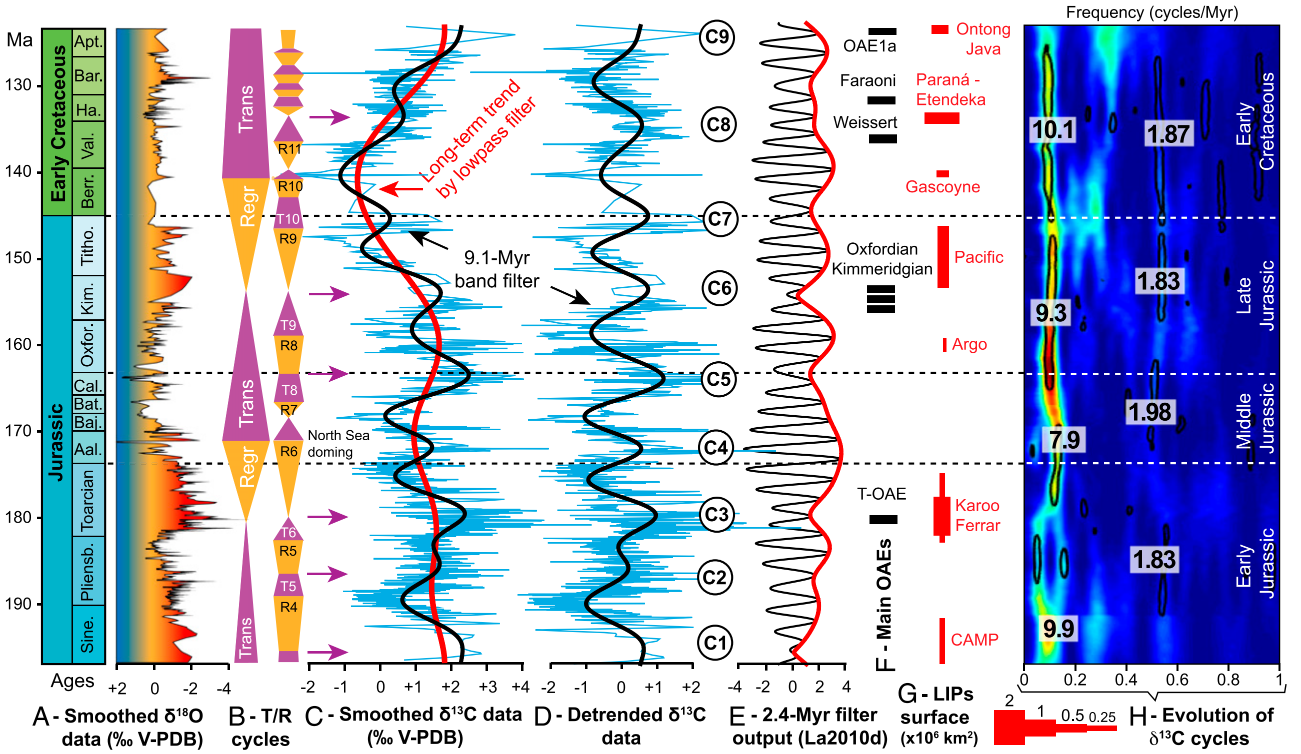

Fig. 3. Comparison of belemnite $\delta^{13}C$ signals with other paleoenvironmental records and astronomical solutions. (*A*) $\delta^{18}O$ time series (this study) reflecting seawater temperature and salinity. (*B*) First-order (*Left*) and second-order (*Right*) cycles of eustatic transgression/regression in the Mediterranean domain (41). (*C*) Belemnite $\delta^{13}C$ time series with Taner low-pass filters showing the general trend (cutoff frequency: 0.04883 cycles per million years, roll-off rate: 10^3) and the 9.1-My cycle (cutoff frequency: 0.1587 cycles per million years, roll-off rate: 10^3). (*D*) Detrended belemnite $\delta^{13}C$ times series with low-pass filter of the 9.1-My cycles numbered from C1 to C9. (*E*) Amplitude modulation of 2.4-My eccentricity cycles showing the ~9-My envelope [calculated from La2010d (4)]. (*F*) Main oceanic anoxic events (56). (*G*) Durations and surface areas of large igneous provinces (56). (*H*) Results from time-frequency Fourier transforms performed with 20-My-width windows showing temporal changes in the expression of the 9.1-My period. The black contours indicate the intervals exceeding the 95% confidence level in the evolutive harmonic F-test. Six positive peaks of $\delta^{13}C$ of nine correspond to maximum flooding events indicated by purple arrows. See Fig. 1 for stratigraphic abbreviations.

Discussion

Orbital Origin of the ~9-My Cycle. The most noticeable result is the detection of an almost continuous cyclicity with a period of 9.1 My in the belemnite $\delta^{13}C$ time series (with a confidence interval ranging from 8.2 to 10.2 My). Combined with previous analyses reporting similar cyclicities of ~8–10 My in the Triassic bedded chert sequences from Japan (8, 15), ~8 My in the Late Cretaceous bulk $\delta^{13}C$ signals from Italy (16), and 8.4 My in the Cenozoic benthic foraminifer $\delta^{13}C$ records from the Pacific (14), this new identification in Jurassic and Early Cretaceous data confirms the presence of periodic changes of ~9 My in the carbon cycle since the beginning of the Mesozoic. Importantly, this pattern would affect both neritic and deep oceanic domains (14). If mainly linked to orbital mechanisms influencing global carbon transfers in response to periodic climate changes, this record throughout the last 230 My represents a challenging constraint for the calibration of next astronomical models, especially in the perspective of discriminating the numerical solutions before 50 Ma and constraining the chaotic diffusion of the solar system in the past (22).

According to astronomical models (La2004 and La2010d) (3, 4) and Cenozoic data (14), the ~9-My cycle modulates the amplitude of the 2.4-My eccentricity cycle. In our study, this hierarchical relationship is difficult to confirm because the low amplitude of the 1.9-My cycle and the lower sampling density from ~160–140 Ma prevent robust AM calculation of this cycle. However, a direct association to the ~9-My eccentricity period is supported by the good match to the theoretical durations (i.e., 9.0 and 9.5 My) inferred from low-frequency AM of the 2.4-My term in the La2004 and La2010d models along the studied interval (Fig. 2*C*). Even if these orbital solutions are not fully reliable for the Mesozoic, the $\delta^{13}C$ data and the AM of the 2.4-My cycles display an antiphased relationship (i.e., maximal $\delta^{13}C$ values during minimal eccentricity) (Fig. 3 *D* and *E*) similar to those observed in the Cenozoic and Late Cretaceous (14, 16, 23). The only exceptions concern the Aalenian cycle C4, which is lacking in orbital solutions, and some inconsistencies between C8 and C9 in the Early Cretaceous, which make the coherency value at 9.1 My high but below the 95% confidence level (Fig. S6).

Contrary to the $\delta^{13}C$ series, the $\delta^{18}O$ data measured on the same belemnites do not record the long eccentricity period of ~9 My, or significant and continuous higher frequency cycles exceeding the Bonferroni-corrected confidence intervals (Fig. 2*B* and Figs. S5 and S7). This is paradoxical because this temperature proxy is generally sensitive to climate changes linked to orbital processes (24). This difference, already observed in conjugate analyses of long-term stable isotope signals (25), likely reflects a decoupling of mechanisms affecting the geochemical expression of the carbon cycle and seawater temperatures during the Mesozoic. The main reason for this mismatch is that the $\delta^{18}O$ signal of belemnites living in neritic domains often reflects a complex message integrating seawater temperature related to climatic conditions but also freshwater influxes, salinity changes, and possible variations in the volume of polar ice caps (26). In addition, the Jurassic and Cretaceous $\delta^{18}O$ variations were not necessarily linked to worldwide climate changes but sometimes influenced by modifications to regional oceanic circulation pathways (27). Consequently, combined processes likely altered the expression of grand orbital cycles in the $\delta^{18}O$ signal.

Disturbance in the ~9-My Cycle. Recurrent disturbances to the carbon cycle from brief volcanic or anoxic events seem not to have measurably affected the long-term sedimentary expression of the underlying eccentricity forcing (Fig. 3 *F* and *G*). However, the ∼9-My cycle displays a quasi-periodic behavior, which questions the factual vs. artificial nature of this irregularity. In the simplest hypothesis, erroneous durations of stages may have distorted the apparent periodicity. For example, the main deviations to the mean periodicity are observed during the Bajocian (i.e., 7.3 My) and the Berriasian–Valanginian (i.e., 11.9 My), whereas new radio- and astrochronological analyses of these intervals report discrepancies of 2–3 My compared with the Geological Time Scale 2012 (GTS 2012) (18, 28). The integration of these new data in the future time scale is therefore of prime importance to better constrain the stability of the ∼9-My cycle during the Mesozoic.

Our analyses also show that the amplitude of the ∼9-My $\delta^{13}C$ cycle decreased from the Pliensbachian to the Early Toarcian (Fig. 3 *D* and *H*). Spectral analyses of bedded cherts from Japan independently report disturbances in an equivalent ∼8- to 10-My cycle from the Hettangian to the Pliensbachian (8, 15) and show that the 2.4-My eccentricity cycle changed between the Rhetian and the Pliensbachian, possibly as the result of chaotic transitions in the Earth–Mars resonance (8). Because the 9-My cycle modulates the 2.4-My eccentricity cycle, this leads to the question of whether the disruption recorded during the Pliensbachian could be linked to chaotic behavior in the solar system. It is difficult to provide a firm answer because, to date, no data confirm a frequency transition in the 9-My cycle. In addition, Japanese data suggest that this disturbance in orbital forcing started much earlier, so that this 25-My-long phenomenon would have exactly prevailed from the Central Atlantic magmatic province flood basalt events to the Karoo–Ferrar eruptions (29) (Figs. 1*B* and 3*G*). Thus, massive injections of volcanic CO_2 into the atmosphere could have destabilized the carbon fluxes over millions of years, which would, in turn, have reduced or dephased the orbital imprint in the $\delta^{13}C$ at million-year time scales.

Amplified Eccentricity Record in the Mesozoic Carbon Cycle. It is surprising that a low-magnitude eccentricity cycle of ∼9 My produces strong amplitudes (i.e., 2‰) in the DIC isotope composition of neritic waters, especially if variations of eccentricity have negligible direct effects on insolation (2). However, because eccentricity modulates the magnitude of precessional changes affecting the seasonal contrast in tropical areas, long eccentricity periods may indirectly pace continental weathering rates, riverine inputs, oceanic fertilization, and alkalinity (23). These processes lead to significant carbon transfers between oceanic, atmospheric, and terrestrial reservoirs (i.e., changes in productivity, organic matter burial or oxidation, and precipitation or dissolution of carbonates) expressed by fluctuations in the $\delta^{13}C$ signal.

A first explanation for the long-term amplification in the carbon cycle could be a "memory" effect produced by the long residence time of carbon in the ocean (i.e., ∼100,000 y), transferring power from high- to low-frequency cycles (9, 30). However, recent mass-balance models suggest that this process alone would be insufficient to amplify the modulation terms at million-year time scales (31). Alternative nonlinear mechanisms could involve cumulative sequestrations of organic carbon in quasi-stable (over millions of years) terrestrial reservoirs from high latitudes (e.g., wetlands, peats, and marginal zones) (31). In this hypothesis, geological periods with greenhouse conditions favoring production and preservation of organic matter (i.e., high pCO_2 levels, warm and equable climates, and high precipitation rates toward high latitudes) should be especially sensitive to eccentricity. According to numerical models and paleobotanical data (32, 33), Jurassic and Early Cretaceous times meet these criteria because mild conditions promoted the development of subtropical plants in most polar domains. By combining our observations to the Cenozoic results of Boulila et al. (14), cumulative organic storage during warm periods explains why the amplitude of ∼9-My $\delta^{13}C$ cycles was maximal (i.e., ∼2‰) from the Jurassic to the Early Eocene, fell to ∼1‰ during the Late Eocene cooling trend, then remained almost stable during the Cenozoic icehouse period.

Climatic and Eustatic Influences of the Eccentricity Forcing. The periodic rises and falls in the $\delta^{13}C$ values suggest that the long eccentricity forcing paced global carbon transfers through eight cycles of organic carbon storage–release throughout the studied interval (i.e., excluding C4) (Fig. 3*D*). From this observation, the causal relationship may be debated in regard to the antiphase of $\delta^{13}C$ data and current eccentricity solutions. In the Mesozoic, periods of maximal eccentricity are often associated with annually dry climates disturbed by short periods of intensive rainfalls and storms, alternatively in the Northern and Southern Hemispheres (16, 23) (Fig. 4*A*). Under arid conditions, the development of vegetation is limited by hydrological stresses, and frequent wildfires

EARTH, ATMOSPHERIC, AND PLANETARY SCIENCES

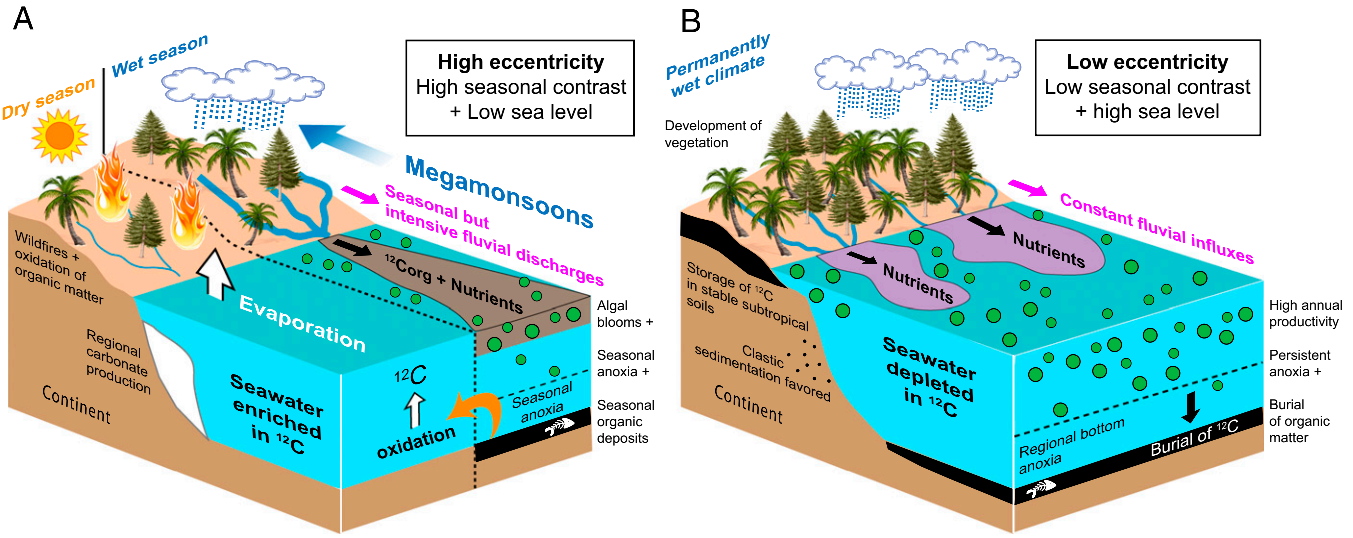

Fig. 4. Scheme of paleoenvironmental changes linked to maxima (*A*) and minima (*B*) of eccentricity. In this model, the carbon cycle is highly influenced by the seasonal dynamics of hydrological processes and sea-level changes.

favor the degradation of organic matter to labile particles (34). Then, monsoonal episodes accelerate continental runoff rates and lead to considerable seasonal fluvial discharges, which stratify the water column and raise the net transfer of nutrients, carbonates, and organic carbon to the ocean (23). The brief but massive input of nutrients fertilizes the oceans and promotes seasonal productivity blooms in poorly mixed waters, which tip the system into anoxia. Nevertheless, this process results in limited organic ^{12}C burial because the recovery of oxic conditions during the cool season degrades the organic particles (35). In agreement with NW Tethyan sedimentary data (36), the absence of organic deposits was locally counterbalanced by high production rates of carbonates, owing to important carbonate influxes and supersaturation under evaporating conditions.

Seasonal oxidation of algal ^{12}C deposits explains the decrease of $\delta^{13}C$ values, but additional factors should be considered. As suggested for the Late Cretaceous (16), considerable fluvial discharges of terrestrial organic carbon (enriched in ^{12}C) during the wet seasons could amplify the geochemical response. Measurements in modern subtropical environments similar to the NW Tethyan area show that 77–92% of the annual budgets of organic carbon are transferred to the sea during the season of tropical cyclones and monsoons (37, 38). Because extreme monsoons linked to significant shifts of the Intertropical Convergence Zone prevailed during the Pangean breakup (33, 39), the terrestrial ^{12}C inputs to the ocean (and their subsequent oxidation) could have been considerable during the phases of maximal eccentricity.

In comparison, eccentricity minima would be characterized by moderate seasonal contrasts in both hemispheres. Even if air temperatures likely fluctuated over the year at the regional scale, climate models of the Late Jurassic suggest that this orbital configuration would have maintained annually wet conditions on the boreal landmasses (33). In agreement, weathering proxies (i.e., $^{87}Sr/^{86}Sr$ or kaolinite inputs) and negative shifts in $\delta^{18}O$ (Fig. 3*A*) indicate that the runoff levels and freshwater inputs raised in the NW Tethyan area during the minimal eccentricity episodes of the Sinemurian, Pliensbachian, Toarcian, and Kimmeridgian (26). This is also confirmed by decreases of seawater εNd values showing that warmer conditions were associated with northward shifts of humid belts weathering the subpolar areas (27). Without arid conditions harmful for the development of vegetation and the preservation of organic matter on continents, or reworking of floodplain organic deposits by exceptional monsoonal events, we propose that annually wet conditions favored the net production of terrestrial biomass (enriched in ^{12}C) and its storage in stable tropical soils of mid and high latitudes (Fig. 4*B*). Additionally, stable and humid conditions on most high-latitude landmasses would have favored constant freshwater and nutrient inputs, water mass stratification, productivity levels, and persistent anoxia. Without seasonal recovery of oxic conditions during the dry season, continuous accumulations of marine organic deposits could partly account for increasing $\delta^{13}C$ values.

Combined with climatic processes, eustatic changes are also involved in the depicted $\delta^{13}C$ fluctuations. This is because flooding (emersion) of continental areas increases (decreases) the surface of marginal domains, and favors higher (lower) marine productivity levels reflected in high (low) seawater $\delta^{13}C$ values in the neritic domains (40). It is worth noting that, among the nine cycles of ∼9 My reported in the $\delta^{13}C$ data, six positive isotopic peaks correspond to maxima of transgression in the second-order sequences (Fig. 3 *B* and *C*) (41), and that these cycles cover a broader isotopic trend globally fitting the first-order sequences in the same way. The three exceptions correspond to the Aalenian, Tithonian–Berriasian, and Aptian periods (cycles C4, C7, and C9), but regional tectonic events (e.g., the North Sea Doming event during the Aalenian) (42) could have hidden the global trend. Overall, because the NW Tethyan passive margin was quite stable, we conclude that the transgressive/regressive cycles and the resulting changes in productivity levels may reflect sea-level changes forced by eccentricity cycles of ∼9 My. Combined with recent identifications of correlations between the ∼2.4-My cycles and the third-order sequences (43), this highlights the importance of orbital eccentricity forcing on sea level at different time scales during the greenhouse periods. Although the exact mechanism remains debated (e.g., groundwater storages) (44), these results strengthen the idea that orbitally paced changes in the hydrological cycle could have been a key factor of eustatic variations during ice-free periods.

Materials and Methods

Data Compilation. We compiled a representative panel of published stable isotope data ($\delta^{13}C$ and $\delta^{18}O$) from the Sinemurian (197.03 Ma) to the Aptian (123.43 Ma). These time series cover 73.6 My and represent a sum of 3,433 and 3,578 data points (Dataset S1), respectively, measured on well-preserved belemnite rostra from European sections. Only belemnites diagenetically screened by cathodoluminescence or geochemical analyses (i.e., low Fe and Mn concentrations), and at least dated at the ammonite biozone resolution, were used for analyses. Although isotope data include different species from different basins, the overall isotopic fluctuations of belemnites match relatively well the variations shown by other organisms such as Jurassic bivalves (26). The stratigraphic position of each isotopic data point was linearly reported to the GTS 2012 (21) at the ammonite (sub)zone level, providing a numerical age (in millions of years ago) for each data point. The resulting time series have an average sample step of 0.04 My and have a much higher resolution than other geochemical compilations based on brachiopods, bivalves, or belemnites from Tethyan domains (25, 26, 45). The more sparsely sampled periods are the Late Kimmeridgian and the Early Berriasian.

Data Preparation. To smooth the time series and to weight the duplicates (i.e., several values for a same age), a robust LOWESS regression was performed on three-age windows (46), representing a coefficient of 0.0016313 and 0.0016667 for the $\delta^{18}O$ and $\delta^{13}C$ time series, respectively. For comparison, the signals were smoothed by calculating the average and median of values having the same age (Fig. S1). Compared with these methods, the LOWESS regression does not affect the result of spectral analyses in densely sampled intervals while reducing the weight of sparsely sampled intervals (Fig. S1). The time series were linearly interpolated at an even step of 0.16 My and the long-term trends were calculated and removed using a Taner low-pass filter (47) with a cutoff frequency of 0.04883 and 0.07324 cycles per million years for the $\delta^{13}C$ and $\delta^{18}O$ series, respectively, and a roll-off rate of 10^3 for both series (Figs. S2 and S3). The series were then standardized (average = 0; SD = 1) and padded to 512 points. Padding to the same number of points allows the series to have the same frequency resolution even after implementation of age uncertainty tests, which modify the length of the series.

Test of Age Uncertainty. The influence of temporal uncertainty, linked to both inaccuracy of the GTS 2012 and temporal positions of data points within ammonite chrons, are tested to confirm the reliability of spectral peaks (Fig. S5). A total of 1,000 Monte Carlo Markov chain (MCMC) simulations of time-scale errors was conducted using the Bayesian Bchron model (48). The MCMC simulations satisfy two conditions: (*i*) The stratigraphic order of data points is respected, and (*ii*) the age variability increases while points are farther from the anchor points (i.e., the stage boundaries and their numerical age uncertainties provided in the GTS 2012). The SD of the offset between the original ages and their corresponding simulated ages is 0.5 My (with 29% of data points having an offset ranging from 0 to ±0.5 My, 95% from 0 to ±1.0 My, and 99.2% from 0 to ±1.5 My) (Fig. S8). The maximal observed offset is ±3.8 My. The R-script for running the age error simulations is available upon request.

Spectral Analysis. A MTM using three 2π-tapers (2π-MTM) was applied to the smoothed series and the 1,000 age-rescaled series (all filtered, detrended, normalized, and padded in the same way) to calculate the most significant periods (49, 50). The frequency uncertainty given in the spectra is assumed to be the Rayleigh frequency of the padded series. The confidence levels were calculated applying the conventional AR1, robust AR1 (51), and LOWSPEC methods (52) with the algorithms available in the astrochron R package (53) (Fig. S4). The thresholds of confidence levels were reappraised using Bonferroni corrections, obtained by dividing the *P* values by the number of positive frequencies explored in the spectral analysis (i.e., 255 frequencies) (54). The nonage randomized time series were submitted to power spectrograms with 20-My window widths to detect temporal changes in the expression of periods (18, 55) (Fig. 3*H* and Fig. S7), and to the F-test and evolutive F-test to determine the purely harmonic or quasi-periodic behavior of main peaks.

ACKNOWLEDGMENTS. We thank Y. Goddéris, H. Johnstone, E. Nardin, H. Pälike, and G. Price for their comments on the early version of the manuscript and L. Hinnov and an anonymous reviewer for their remarks, which helped improve the results. The Anox-Sea National Research Agency and EARTHSEQUENCING European Research Council Consolidated Grant projects financed this work.

1. Berger A, Loutre MF (1994) Precession, eccentricity, obliquity, insolation and paleoclimates. Long-term Climatic Variations, NATO ASI Series, eds Duplessy JC, Spyridakis MT (Springer, Berlin), Vol 22, pp 107–151.
2. Paillard D (2010) Climate and the orbital parameters of the Earth. *C R Geosci* 342(4-5): 273–285.
3. Laskar J, et al. (2004) A long-term numerical solution for the insolation quantities of the Earth. *Astron Astrophys* 428:261–285.
4. Laskar J, Fienga A, Gastineau M, Manche H (2011) La2010: A new orbital solution for the long-term motion of the Earth. *Astron Astrophys* 532:A89.
5. Hinnov LA (2013) Cyclostratigraphy and its revolutionizing applications in the earth and planetary sciences. *Geol Soc Am Bull* 125(11-12):1703–1734.
6. Olsen PE (2001) Grand cycles of the Milankovitch Band. *Eos Trans Am Geophys Union* 47(Suppl 82):F2 (abstr).
7. Laskar J (1990) The chaotic motion of the solar system: A numerical estimate of the size of the chaotic zone. *Icarus* 88(2):266–291.
8. Ikeda M, Tada R (2013) Long period astronomical cycles from the Triassic to Jurassic bedded chert sequence (Inuyama, Japan); Geologic evidences for the chaotic behavior of solar planets. *Earth Planets Space* 65(4):351–360.
9. Pälike H, et al. (2006) The heartbeat of the Oligocene climate system. *Science* 314(5807):1894–1898.
10. Wu H, et al. (2013) Time-calibrated Milankovitch cycles for the late Permian. *Nat Commun* 4:2452.
11. Boulila S, et al. (2010) Milankovitch and sub-Milankovitch forcing of the Oxfordian (Late Jurassic) Terres Noires Formation (SE France) and global implications. *Basin Res* 22(5):717–732.
12. Huang C, Hinnov LA, Fischer AG, Grippo A, Herbert T (2010) Astronomical tuning of the Aptian Stage from Italian reference sections. *Geology* 38(10):899–902.
13. Olsen PE, Kent DV (1999) Long-period Milankovitch cycles from the Late Triassic and Early Jurassic of eastern North America and their implications for the calibration of the Early Mesozoic time-scale and the long-term behaviour of the planets. *Philosophical Transactions of the Royal Society A* 357(1757):1761–1786.
14. Boulila S, Galbrun B, Laskar J, Pälike H (2012) A ~9 myr cycle in Cenozoic $\delta^{13}C$ record and long-term orbital eccentricity modulation: Is there a link? *Earth Planet Sci Lett* 317—318:273–281.
15. Ikeda M, Tada R (2014) A 70 million year astronomical time scale for the deep-sea bedded chert sequence (Inuyama, Japan): Implications for Triassic–Jurassic geochronology. *Earth Planet Sci Lett* 399:30–43.
16. Sprovieri M, et al. (2013) Late Cretaceous orbitally-paced carbon isotope stratigraphy from the Bottaccione Gorge (Italy). *Palaeogeogr Palaeoclimatol Palaeoecol* 379–380: 81–94.
17. Huang CJ, Hesselbo SP, Hinnov L (2010) Astrochronology of the late Jurassic Kimmeridge Clay (Dorset, England) and implications for Earth system processes. *Earth Planet Sci Lett* 289(1-2):242–255.
18. Martinez M, et al. (2015) Astrochronology of the Valanginian-Hauterivian stages (Early Cretaceous): Chronological relationships between the Paraná-Etendeka large igneous province and the Weissert and Faraoni events. *Global Planet Change* 131: 158–173.
19. Mutterlose J, Malkoc M, Schouten S, Sinninghe Damsté JS, Forster A (2010) Tex86 and stable $\delta^{18}O$ paleothermometry of early Cretaceous sediments: Implications for belemnite ecology and paleotemperature proxy application. *Earth Planet Sci Lett* 298(3-4):286–298.
20. Ullmann CV, Thibault N, Ruhl M, Hesselbo SP, Korte C (2014) Effect of a Jurassic oceanic anoxic event on belemnite ecology and evolution. *Proc Natl Acad Sci USA* 111(28):10073–10076.
21. Gradstein FM, Ogg JG, Schmitz MD, Ogg GM (2012) *The Geologic Time Scale 2012* (Elsevier, Amsterdam).
22. Pälike H, Laskar J, Shackleton NJ (2004) Geologic constraints on the chaotic diffusion of the solar system. *Geology* 32(11):929–932.
23. Ma W, Tian J, Li Q, Wang P (2011) Simulation of long eccentricity (400-kyr) cycle in ocean carbon reservoir during the Miocene Climate Optimum: Weathering and nutrient response to orbital change. *Geophys Res Lett* 38(38):L10701.
24. Zachos J, Pagani M, Sloan L, Thomas E, Billups K (2001) Trends, rhythms, and aberrations in global climate 65 Ma to present. *Science* 292(5517):686–693.
25. Prokoph A, Shields GA, Veizer J (2008) Compilation and time-series analysis of a marine carbonate $\delta^{18}O$, $\delta^{13}C$, $^{87}Sr/^{86}Sr$ and $\delta^{34}S$ database through Earth history. *Earth Sci Rev* 87(3):113–133.
26. Dera G, et al. (2011) Climatic ups and downs in a disturbed Jurassic world. *Geology* 39(3):215–218.
27. Dera G, et al. (2015) Nd isotope constraints on ocean circulation, paleoclimate, and continental drainage during the Jurassic breakup of Pangea. *Gondwana Res* 27(4): 1599–1615.
28. Suchéras-Marx B, et al. (2013) Duration of the Early Bajocian and the associated $\delta^{13}C$ positive excursion based on cyclostratigraphy. *J Geol Soc London* 170(5):107–118.
29. Prokoph A, El Bilali H, Ernst R (2013) Periodicities in the emplacement of large igneous provinces through the Phanerozoic: Relations to ocean chemistry and marine biodiversity evolution. *Geoscience Frontiers* 4(3):263–276.
30. Cramer BS, Wright JD, Kent DV, Aubry MP (2003) Orbital climate forcing of $\delta^{13}C$ excursions in the late Paleocene-early Eocene (chrons C24n-C25n). *Paleoceanography* 18:1097.
31. Laurin J, Meyers SR, Uličný D, Jarvis I, Sageman BB (2015) Axial-obliquity control on the greenhouse carbon budget through mid- to high-latitude reservoirs. *Paleoceanography* 30:133–149.
32. Rees PM, Ziegler AM, Valdes PJ (2000) Jurassic phytogeography and climate: New data and model comparisons. *Warm Climates in Earth History*, eds Huber BT, Macleod KG, Wing SL (Cambridge Univ Press, Cambridge, UK), pp 297–318.
33. Valdes PJ, Sellwood BW, Price GD (1995) Modelling Late Jurassic Milankovitch climate variations. *J Geol Soc* 85(Special Publications):115–132.
34. Matthewmann R, Cotton LJ, Martins Z, Sephton MA (2012) Organic geochemistry of late Jurassic paleosols (Dirt Beds) of Dorset, UK. *Mar Pet Geol* 37(1):41–52.
35. Capet A, Beckers JM, Grégoire M (2013) Drivers, mechanisms and long-term variability of seasonal hypoxia on the Black Sea northwestern shelf—Is there any recovery after eutrophication? *Biogeosciences* 10:3943–3962.
36. Brigaud B, et al. (2014) Growth and demise of the Jurassic carbonate platform in the intracratonic Paris Basin (France): Interplay of climate change, eustasy and tectonics. *Mar Pet Geol* 53:3–29.
37. Hilton RG, et al. (2008) Tropical-cyclone driven erosion of the terrestrial biosphere from mountains. *Nat Geosci* 1:759–762.
38. Honjo S, Dymond J, Prell W, Ittekkot V (1999) Monsoon-controlled export fluxes to the interior of the Arabian Sea. *Deep Sea Res Part II Top Stud Oceanogr* 46(8-9): 1859–1902.
39. Crowley TJ, Baum SK, Hyde WT (1992) Milankovitch fluctuations on supercontinents. *Geophys Res Lett* 19(8):793–796.
40. Jarvis I, Mabrouk A, Moody RTJ, de Cabrera S (2002) Late Cretaceous (Campanian) carbon isotope events, sea-level changes and correlation of the Tethyan and Boreal realms. *Palaeogeogr Palaeoclimatol Palaeoecol* 188(3-4):215–248.
41. Hardenbol J, Thierry J, Farley MB, de Graciansky P-C, Vail PR (1998) Mesozoic and Cenozoic sequence chronostratigraphic framework of European basins. *Mesozoic and Cenozoic Sequence Stratigraphy of European Basins*, eds de Graciansky P-C, Hardenbol J, Jacquin T (Society for Sedimentary Geology, Tulsa, OK), Vol 60, pp 3–13.
42. Hallam A (2001) A review of broad pattern of Jurassic sea-level changes and their possible causes in the light of current knowledge. *Palaeogeogr Palaeoclimatol Palaeoecol* 167(1-2):23–37.
43. Boulila S, et al. (2011) On the origin of Cenozoic and Mesozoic "third-order" eustatic sequences. *Earth Sci Rev* 109(3-4):94–112.
44. Hay WW (2008) Evolving ideas about the Cretaceous climate and ocean circulation. *Cretac Res* 29(5-6):725–753.
45. Price GD, Twitchett RJ, Wheeley JR, Buono G (2013) Isotopic evidence for long term warmth in the Mesozoic. *Sci Rep* 3:1438.
46. Cleveland WS (1979) Robust locally weighted regression and smoothing scatterplots. *J Am Stat Assoc* 74(368):829–836.
47. Taner MT (2000) *Attributes Revisited* (Rock Solid Images, Inc., Houston, TX).
48. Parnell AC, Haslett J, Allen JRM, Buck CE, Huntley B (2008) A flexible approach to assessing synchroneity of past events using Bayesian reconstructions of sedimentation history. *Quat Sci Rev* 27(19-20):1872–1885.
49. Thomson DJ (1982) Spectrum estimation and harmonic-analysis. *Proc IEEE* 70: 1055–1096.
50. Thomson DJ (1990) Quadratic-inverse spectrum estimates—Applications to paleoclimatology. *Philos Trans R Soc A* 332(1627):539–597.
51. Mann ME, Lees JM (1996) Robust estimation of background noise and signal detection in climatic time series. *Clim Change* 33(3):409–445.
52. Meyers SR (2012) Seeing red in cyclic stratigraphy: Spectral noise estimation for astrochronology. *Paleoceanography* 27:PA3228.
53. Meyers SR (2014) Astrochon: An R package for astrochronology. Available at cran.r-project.org/web/packages/astrochron/index.html.
54. Dunn OJ (1961) Multiple comparisons among means. *J Am Stat Assoc* 56(293):52–64.
55. Park J, Lindberg CR, Vernon FL (1987) Multitaper spectral analysis of high-frequency seismograms. *J Geophys Res* 92(B12):12675–12684.
56. Trabucho-Alexandre J, Hay WW, de Boer PL (2012) Phanerozoic environments of black shale deposition and the Wilson Cycle. *Solid Earth* 3:29–42.
57. Thierry J, et al. (2000) Middle Toarcian. *Atlas peri-Tethys, Palaeogeographical maps*, eds Dercourt J, et al. (Commission of the Geological Map of the World, Paris), Map 8.